DESIGN OF AN EXPERIMENTAL SET-UP TO ANALYSE COMPLIANT MECHANISMS USED FOR THE DEPLOYMENT OF A PANEL

Florence Dewalque, Olivier Brüls

Department of Aerospace and Mechanical Engineering, University of Liège
Allée de la Découverte 9 (B52/3), 4000 Liège, Belgium
`f.dewalque@ulg.ac.be`

Abstract

Due to their high complexity, compliant mechanisms require high-fidelity mechanical models to reach a detailed understanding of their characteristics and predict their actual behaviour in various situations. This work focuses on tape springs which are used as an alternative to common mechanisms composed of kinematic joints. They present several assets such as, among others, passive deployment and self-locking, but they are characterised by a highly nonlinear behaviour including buckling, the formation of folds and hysteresis. An experimental set-up is then designed to gather information on these phenomena, while in parallel an equivalent finite element model is developed. Quasi-static and dynamic tests are performed, as well as small amplitude vibration tests and large amplitude deployments in order to collect data in a broad variety of cases. The post-processing of the numerous raw data shows, with the help of statistical considerations, the good quality of the acquisitions. Finally, the finite element model proves to be fairly well correlated to the experimental results.

1 INTRODUCTION

The development of low cost missions requires the use of simple, robust and easy-to-integrate components in order to reduce both the time-consuming period of numerical and experimental tests and the subsequent manufacturing cost of spacecraft. In order to meet these objectives in the domain of space deployable structures, the common mechanisms, usually composed of several kinematic joints which are set into motion by the means of motors, can be replaced by autonomous compliant elements. In this work, the characteristics of tape springs, belonging to the second category of mechanisms, will be analysed through the design of an experimental set-up.

Tape springs have already been successfully used in several space missions such as the six MYRI-ADE micro-satellites for the deployment of solar arrays, antennas and masts [1] or the MARS EXPRESS spacecraft for the deployment of a long wavelength antenna [2] and will be used in future missions such as SOLAR ORBITER for the deployment of a radio and plasma wave antenna or NORSAT-1 for the deployment of an AIS receiver. Indeed, the inherent characteristics of tape springs turn out to show many advantages for space deployable structures. First of all, when a tape spring is deformed to reach its folded configuration, the deformations stay in the elastic regime, provided that the geometric and material parameters satisfy a design constraint [3]. The stored

elastic energy is then responsible for a residual moment that leads to a passive and self-actuated deployment until the tape spring reaches its equilibrium state which, in the context of this work, is the straight configuration, even though another one may exist [4]. Furthermore, compared to kinematic joints which usually imply some sliding between contact surfaces while in motion, the deployment of tape springs only leads to the deformation of structural elements. The use of lubricant is then irrelevant in this case and the risks of outgassing or contamination are limited. Finally, several tape springs can easily be combined to form a hinge with characteristics specific to the application at hand, showing thus the versatility of these mechanisms. For example, the MAEVA hinge is composed of three tape springs with alternate orientations [5], Boesch *et al.* designed a hinge with four pairs of tape springs, each composed of a long and a short element [6]. The assets of tape springs can also be found in hinges consisting of thin walled tubes with two symmetric longitudinal holes along a chosen region which results in two superimposed tape springs with opposite curvatures also called integral slotted hinges [2, 7].

The advantageous characteristics of tape springs result from their highly nonlinear mechanical behaviour which is theoretically illustrated in Fig. 1 and describes the evolution of the bending moment M measured at the clamped extremity of the tape spring when the bending angle θ is controlled at the other

end. First of all, the sense of bending has a significant impact on the behaviour and on the deformed configuration of the tape spring. The two senses of bending are called and described as follows: the opposite sense bending $(M, \theta > 0)$ leads to longitudinal and transverse curvatures in opposite sense, while the equal sense bending $(M, \theta < 0)$ leads to longitudinal and transverse curvatures in the same sense. In opposite sense, after first increasing linearly and reaching a maximum M_+^{max}, the loading curve undergoes a sharp drop which is due to the buckling of the structure and leads to the formation of a fold in the middle of the tape spring. In this configuration, the regions away from the fold remain straight and can easily be moved until they are parallel to each other since the residual moment M_+^* is much smaller than the maximum M_+^{max}. Furthermore, in the case where the two extreme regions are parallel, the gap between the two sides reaches approximately twice the transverse radius of the tape spring in its equilibrium state [8] and shows that a compact folded configuration can be achieved. During the unloading stage, the fold disappears for an angle θ_+^{heel} smaller than the one associated to buckling. This non-superposition of the loading and unloading paths is responsible for an hysteresis phenomenon which leads to a dissipation of energy and, in the end, to the self-locking of the structure in its deployed configuration. On the other hand, the equal sense bending is also characterised by the formation of a transverse fold which results from the combination of torsion folds starting from the extremities and converging to the middle as the amplitude of the bending angle increases. This evolution being more progressive than in opposite sense, the maximum and residual moments are smaller in amplitude than their opposite sense counterparts ($|M_-^{max}| < M_+^{max}$, $|M_-^*| < M_+^*$). Finally, it is commonly accepted in theory that the cycles of loading-unloading are superimposed in equal sense bending even though it is not exactly the case in practice [9].

Due to the high complexity of the tape spring behaviour, high-fidelity mechanical models are required to accurately predict their evolution in various applications. To this end, analytical development, finite element analyses and experimental tests are performed. The theoretical relationship illustrated in Fig. 1 was first derived by Wüst [10], Rimrott [11] and Mansfield [12]. Analytically, the deployment of tape springs is usually described with the help of simplifying assumptions. For example, since the fold after buckling is localised and the regions near the extremities remain straight, a tape
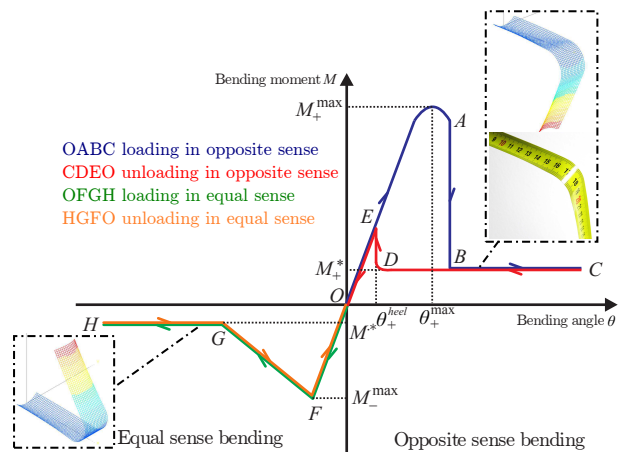

Figure 1: Theoretical evolution of the bending moment M with respect to the bending angle θ in pure bending (inspired from [3]).

spring can be represented by a mobile hinge connecting two rigid bodies of variable length [9] or by a one-dimensional planar rod with flexible cross-sections [13]. Regarding finite element models, comprehensive quasi-static analyses were performed in order to understand the impact of the geometric and material parameters on the relationship linking the bending moment M and the bending angle θ in the case of a single tape spring [3, 14] or integral slotted hinges [17] and nonlinear dynamic analyses were performed to capture the phenomena (buckling, hysteresis, self-locking) characterising the deployment of tape springs [15, 16].

Experimental tests, usually combined to finite element models used for the initial design or the correlation of the full deployment simulation, can be found in [9, 19] for single tape springs, in [5, 6, 20] for hinges composed of multiple tape springs, in [2, 17] for the deployment of integral slotted hinges and in [18] where tape springs are used as structural stiffeners for inflatable structures. With current finite element software, fair correlations are obtained between the experimental and numerical results. However, one parameter remains challenging to experimentally determine and integrate in a finite element model: the structural damping. A previous work [16] showed that this physical property is required to ensure a correct representation of the damping of the oscillations after deployment and of the self-locking phenomenon of the tape springs in their equilibrium state, and led to more robust simulations by reducing the sensitivity of the numerical models to the numerical dissipation of the transient solver. Some works already integrate structural damping in their finite element models by the means of proportional damping with either constant damping factors [21] or vari-

able ones based on the natural frequency of the tape spring hinge [2] or by fitting Prony series [22]. In this work, an experimental set-up is designed in order to gather information on the structural damping by submitting the structure to small amplitude vibrations, the decrease of which allows completing and verifying the numerical results obtained in [16] where the structural damping was represented by a Kelvin-Voigt model. Furthermore, quasi-static and passive deployment tests are performed on this experimental set-up to collect data in the case of large amplitude motions. Finally, in parallel to these tests, a finite element model is correlated to the experimental results in order to ensure the reliability of the numerical results in further applications.

The layout of this paper is as follows. The design of the experimental set-up is described in Section 2. Then, in Section 3, three points bending tests are performed in order to reduce the uncertainties affecting the values of the Young's modulus E and the thickness t. The last unknown parameter, the structural damping ε, is experimentally evaluated by the means of small amplitude vibration tests in Section 4. In Section 5, deployment tests are performed in order to collect data on large amplitude motions. Finally, the conclusions of this work are drawn in Section 6.

2 EXPERIMENTAL SET-UP

The experimental set-up is schematically illustrated in Fig. 2. The hinge is composed of two tape springs cut out at the required length from a common measuring tape as the one visible in Fig. 1. They have the same orientation so that the initial bending prior to deployment can be performed in opposite or equal sense by turning upside down the whole block composed of the tape springs, the interfaces and the dummy appendix. Each extremity of the tape springs is clamped by interfaces (Fig. 2c) composed of two complementary parts with curved regions fitting the geometry of the tape springs.

The different parameters of this latter are given in Tab. 1 and illustrated in Fig. 2c. Only the length L, the thickness t, the width w and the height h were physically measured using a calliper, while the subtended angle α and the radius of curvature R were calculated based on these parameters with the help of simple trigonometric equations. Regarding the length L, the given value corresponds to the distance between the two faces of the interfaces facing each other (Fig. 2b), that is without the parts of the tape springs clamped in the interfaces.

Some uncertainties affect the value of the thickness t. Indeed, its size is one to three orders of mag-

$L\ [mm]$	$t\ [mm]$	$w\ [mm]$	$h\ [mm]$	$\alpha\ [°]$	$R\ [mm]$
100	~ 0.14	17.8	2.8	69.85	15.545

Table 1: Geometric characteristics of the tape springs used in the experimental set-up.

nitude smaller than all the other dimensions of the tape springs, which makes it more complex to accurately measure. Furthermore, since the tape springs are parts of a common measuring tape, they consist of a metallic layer covered by a wear resistant coating and surrounded on both faces by protective layers of transparent plastic. It can then be expected from this that the distribution of the thickness is not constant along the length and the width of the tape spring. A measurement of an uneven distribution of thickness can be found in [22] even though the tape springs were manufactured with a single polymeric material. All these elements lead to an approximated value of thickness t given in Tab. 1, but also to an unknown value for the Young's modulus E. In order to determine these two parameters, specific experimental tests are performed further in this work.

The interfaces clamping the tape springs are connected on one side to a fixation support considered as clamped to the ground due to its own weight and to a dummy appendix on the other one. One objective is to study an autonomous deployment of the appendix despite the presence of the gravity field. It implies that when designing the experimental set-up, one must ensure that the weight at the free end (the combination of two interfaces and the dummy appendix) is limited in order to respect two constraints. First of all, the structure cannot buckle under its own weight, and secondly, when initially folded downwards, the residual moment in the tape springs must be able to passively deploy the structure until the equilibrium state is recovered. As it can be deduced from the quasi-static relationship between the bending angle θ and the resulting bending moment M (Fig. 1), the second constraint is the most restrictive one since the residual moment M^* is smaller than the maximum moment M^{max} right before buckling, whatever the sense of folding. Furthermore, as explained previously, the amplitude of the residual moment is smaller in equal sense. It implies then that in order to use the same set-up in both senses, the maximum weight is fixed by the behaviour in equal sense bending.

Taking into account these restrictions regarding the mass, the designed experimental set-up is given in Fig. 3. In total, the two interfaces, the rod and the dummy appendix have a mass of $\sim 77\ g$. Notice that

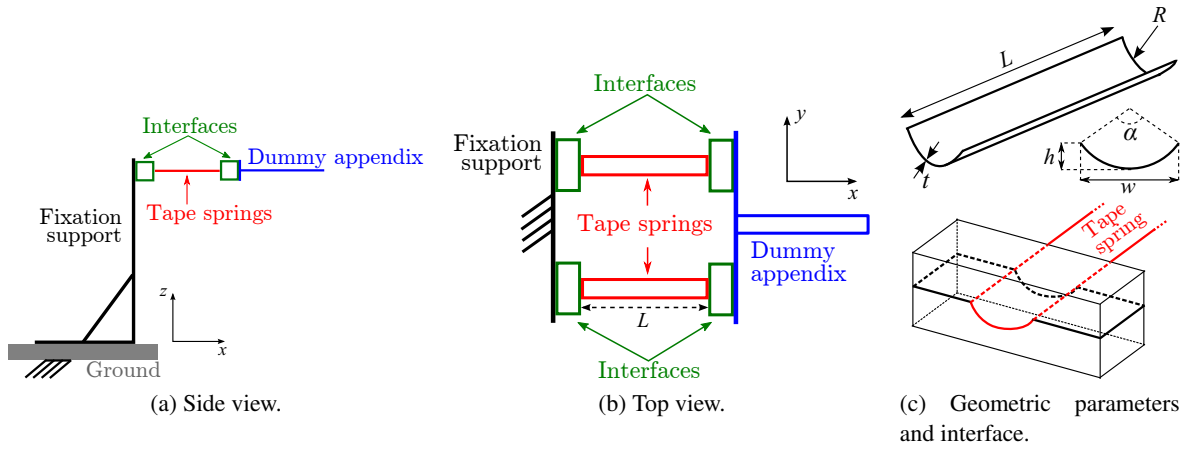| (a) Side view. | (b) Top view. | (c) Geometric parameters and interface. |

Figure 2: Schematic representation of the experimental set-up.

to achieve this low mass, it was necessary to clamp the interfaces around the tape springs free ends by the means of only one screw, which implies that it goes through the tape springs, and to drill additional holes in the rod and the dummy appendix. In the case of the interfaces connecting the tape springs to the fixation support, larger ones are used since their weight does not affect the deployment.
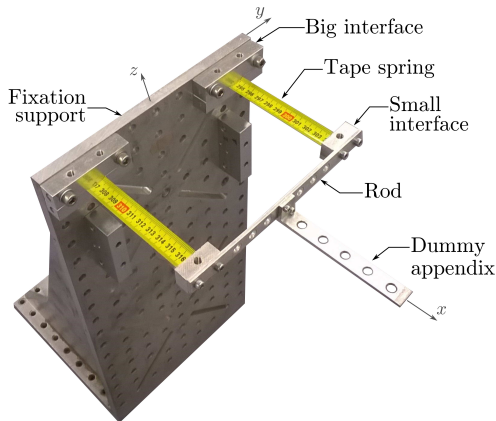
Figure 3: Experimental set-up.
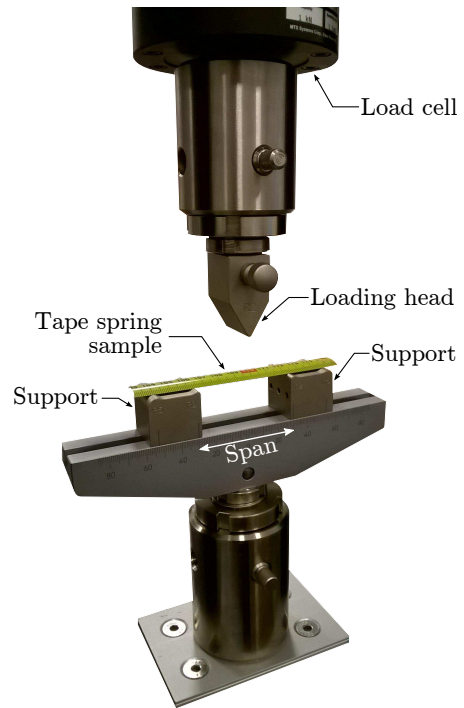
Figure 4: Experimental three points bending test.

3   THREE POINTS BENDING TESTS

In order to reduce the uncertainties on the Young's modulus E and the thickness t, three points bending tests are performed. The test consists of a loading head coming into contact with a tape spring sample positioned on two supports separated by a chosen span (Fig. 4). The machine used is a MTS CRITERION with a load cell of 1 kN, the tip of the loading head and the corners of the supports have a radius of 2 mm, and the span is set to 60 mm.

For each tape spring, ten tests are performed in the two senses of bending. The results obtained on one

sample are illustrated in Fig. 5 where the 20 curves (10 in opposite sense and 10 in equal sense) are superimposed and show a good reproducibility. Notice that this evolution is different from the theoretical one described in Fig. 1, since three points bending tests give the relationship between the load and the displacement of the head, instead of the bending moment with respect to the bending angle. Nonetheless, the same main characteristics are identified: for small displacements, the evolution is first linear; then a maximum is reached, the amplitude being smaller in equal sense; it is followed by buckling which is

sharper in opposite sense; and finally large displacements are associated to a residual load.
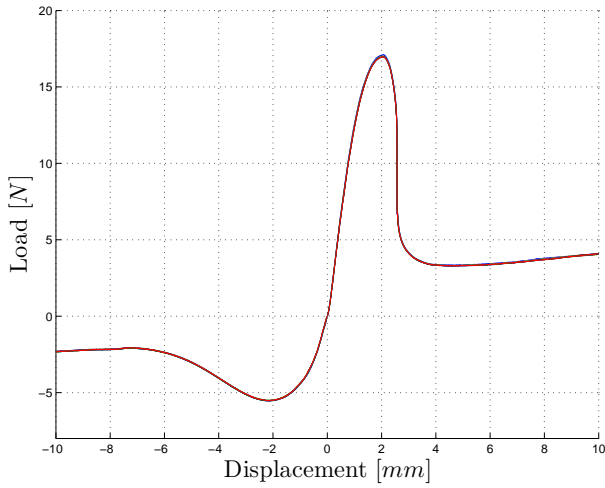

Figure 5: Experimental results of the three points bending tests for a single tape spring (10 curves in opposite sense and 10 curves in equal sense).

Regarding the reproducibility of the tests for different tape springs, the results are given in Tabs. 2 and 3 where three features are considered: the maximum load, the associated displacement of the loading head and the slope for small displacements. In each case, the mean value of all the tests (in total, 6 tape springs were used, so that each mean is computed on 60 values) is given, along with the largest difference noticed within the results and the associated variation coefficient. This latter, also called relative standard deviation, measures the dispersion of the results and is defined as the ratio between the standard deviation and the mean. It is used here to evaluate the accuracy and the repeatability of the measures and is expressed as a percentage. As the variation coefficient remains below 5 % for each feature, it can be concluded that these experimental tests also show a good reproducibility from one tape spring to another. The only noticeable sources of errors during the tests came from a bad alignment of the tape spring with respect to the loading head and the supports or a bad tightening of the loading head in the load cell, which can be both easily avoided by carefully preparing the set-up.

| | Opposite sense | | |
	Mean	Max. diff.	Variation coeff.
Max. load [N]	17.46	0.97	1.77 %
Disp. [mm]	2.04	0.32	4.04 %
Slope [N/mm]	12.76	0.96	1.86 %

Table 2: Experimental results from the three points bending tests in opposite sense.

| | Equal sense | | |
	Mean	Max. diff.	Variation coeff.
Max. load [N]	5.53	0.36	1.46 %
Disp. [mm]	2.17	0.33	3.72 %
Slope [N/mm]	6.94	1.25	4.85 %

Table 3: Experimental results from the three points bending tests in equal sense.

In order to determine the values of the Young's modulus E and the thickness t which lead to these experimental results, finite element models reproducing the three points bending tests are used. In this work, all the finite element models are developed in the commercial software SAMCEF [23]. More precisely, the tape springs are represented by flexible shell elements base on the Mindlin-Reissner theory, since as already mentioned their thickness is several orders of magnitude smaller than their other dimensions. The loading head and the supports are simplified as cylinders with a radius of 2 mm, since contact only occurs on the tip and the corners of these elements. Furthermore, they are all three considered as rigid, while the tape spring is obviously flexible. Regarding contact, a coupled iterations method is exploited, meaning that contact is treated as a nonlinearity and a kinematic constraint is active when contact occurs and inactive otherwise. Finally, the supports are considered as fixed, while the displacement of the loading head is controlled. The resulting deformed configurations in both senses obtained with these models are given in Fig. 6 where the Newmark method [24] was exploited to solve this nonlinear problem with an adaptive time stepping procedure. In opposite sense, the model stops converging right after reaching the maximum load and is unable to capture buckling, while in equal sense it succeeds since this phenomenon is less sharp.
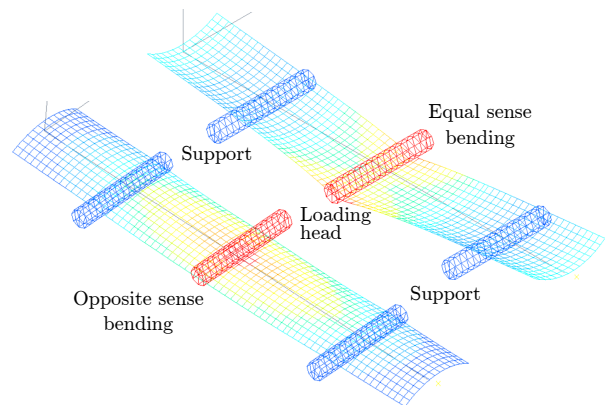

Figure 6: Finite element models for the three points bending tests (deformed configurations).

The finite element models are integrated in an op-

timisation procedure that will lead to the Young's modulus E and the thickness t fitting at best the previous experimental results. The generic form of an optimisation problem is expressed as:

$$\min_{x} f(x) \text{ such that } \begin{cases} c(x) \leq 0 \\ lb \leq x \leq ub \end{cases} \quad (1)$$

where $f(x)$ is the objective function to be minimised with respect to the vector of design variables x, $c(x)$ represents the nonlinear inequality constraints, and lb and ub are vectors defining respectively the lower and upper bounds of the design variables.

In this case, the design variables are the Young's modulus E, the thickness t and the friction coefficient μ between the tape spring and the loading head and supports. This latter is not required for the small amplitude vibration tests or deployment tests, nonetheless it affects the results of the three points bending tests as it can be seen in Fig. 7. To simplify the problem, it is assumed that the friction coefficient μ is the same at the three contact locations.
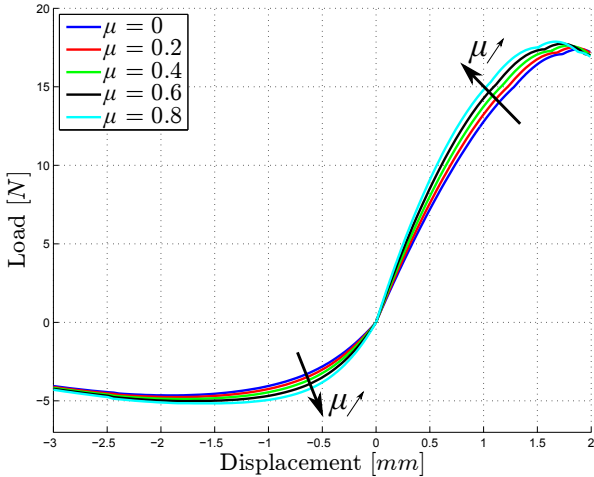

Figure 7: Impact of the friction coefficient μ on the three points bending tests.

The function to be minimised quantifies the correlation between the numerical and the mean experimental results. To this end, the loads are compared at four specific displacements: the ones associated to the maximum loads and at a displacement of 1 *mm* in both senses. The objective function $f(x)$ is then the sum of the differences, each term being divided by the corresponding mean experimental value in order to sum terms with the same order of magnitude.

Regarding the constraints, only bounds limit the values of the design variables and are defined in Tab. 4. For the Young's modulus E and the thickness t, ranges of values allowing a passive deployment of the mass at the free extremities of the tape

springs determined in Section 2 are used, while limitations concerning the convergence of the finite element models lead to the bounds of the friction coefficient μ. For information, an optimisation procedure using nonlinear inequality constraints can be found in [14].

Bounds	$E\ [MPa]$	$t\ [mm]$	$\mu[-]$
lb	100000	0.12	0
ub	220000	0.2	0.8

Table 4: Lower and upper bounds of the design variables in the three points bending tests.

The problem is solved by the means of the interior-point algorithm available through the `fmincon(...)` function in MATLAB which solves large, sparse multivariable problems, as well as small dense ones [25]. The termination tolerance on the objective function and the design variables, and the tolerance on the constraint violation are all set to 10^{-3}. The result of such optimisation procedure is a local minimum of the objective function. It is then dependent on the initial guess and usually several tests have to be performed before finding a global solution.

The optimisation procedure is as follows (Fig. 8). Starting from an initial guess (E_0, t_0, μ_0), the three points bending tests are numerically performed in both senses by the means of the finite element models described in Fig. 6. The results are post-treated in order to extract the evolution of the load with respect to the displacement of the loading head. Then, the objective function is computed and the validity of the constraints is checked in the optimisation routine. If the value of the objective function is minimised, the solution of the problem $(E_{end}, t_{end}, \mu_{end})$ is found, otherwise the algorithm determines automatically the next set of design variables (E_k, t_k, μ_k) and a new cycle of analyses is carried out.

The results of the optimisation procedure regarding the Young's modulus E, the thickness t and the friction coefficient μ are given in Tab. 5. A comparison with the experimental results is illustrated in Fig. 9 where it can be seen that visually the main difference comes from the amplitude of the maximum load in opposite sense. Nonetheless, by comparing quantitatively the four loads defining the objective function, Tabs. 6 and 7 show a good agreement between the numerical and experimental results, a larger difference being notice at the maximum load in opposite sense, while it is for a displacement of -1 *mm* in equal sense.

For information, tensile tests were also attempted to determine the values of the Young's modulus E
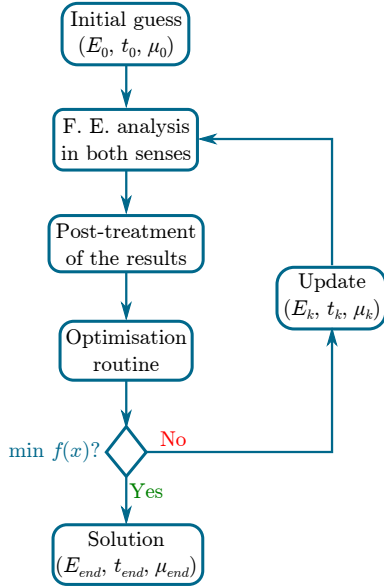
Figure 8: Optimisation procedure to correlate the results from the three points bending tests.

$E\ [MPa]$	$t\ [mm]$	$\mu[-]$
187812	0.132	0.218

Table 5: Results of the optimisation procedure for the three points bending tests.
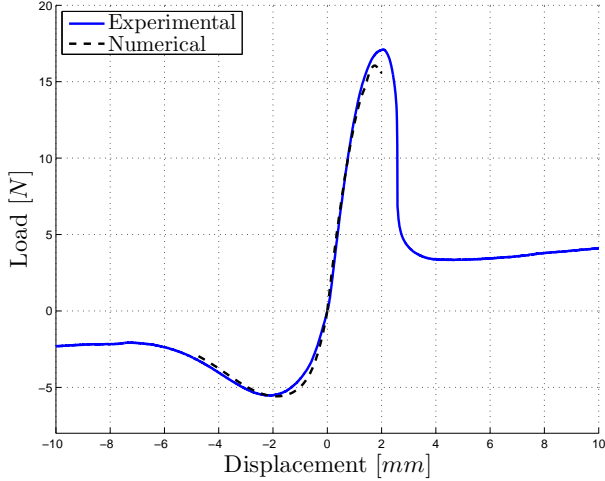

Figure 9: Graphical comparison between the results of the optimisation procedure for the three points bending tests and one experimental curve.

and the thickness t, but were inconclusive. In order to keep the geometry of the tape springs unconstrained, mechanical interfaces were used at each of their extremities and the grips of the machine were clamping these interfaces. However, they were either slipping between the grips or the tape springs were breaking inside the interfaces with the crack starting at the hole dedicated to the screw.

	Opposite sense	
	Max. load $[N]$	Load at 1 mm $[N]$
Exp.	17.46	12.38
Num.	15.61	12.02
Δ	10.60 %	2.91 %

Table 6: Comparison between the experimental results and the optimisation procedure for the three points bending tests in opposite sense.

	Equal sense	
	Max. load $[N]$	Load at -1 mm $[N]$
Exp.	5.53	4.34
Num.	5.55	4.94
Δ	0.36 %	13.82 %

Table 7: Comparison between the experimental results and the optimisation procedure for the three points bending tests in equal sense.

4 SMALL AMPLITUDE VIBRATION TESTS

Now that the uncertainties on the Young's modulus E and the thickness t are reduced, the next physical parameter to determine is the structural damping ε. As mentioned in the introduction, it was shown in a previous work [16] that the structural damping ε only affects the low frequency domain of a structure, while the numerical damping is used to filter the high frequency modes poorly represented in the discretised finite element models. It improves thus the convergence of the solver, especially for nonlinear structures. Furthermore, the structural damping ε is required to capture the damping of the small amplitude oscillations after deployment and the self-locking of the tape springs in their deployed state. Finally, more robust simulations are obtained since introducing some structural damping in the models reduces the sensitivity of the results to the amount of numerical damping.

The structural damping is a physical property of the material composing the tape springs. However, additional sources of damping are present in the experimental set-up due to loses at the connections between each element, to the flexibility of other components which are also characterised by a certain amount of structural damping, to the air resistance as the tests are not performed in vacuum or to acoustic effects which can be heard every time a fold is formed or disappears. Thus, the structural damping coming from the tape springs cannot be easily isolated from all the other sources of dissipation and the experimental measures give only general information on the behaviour of the whole structure.

In order to evaluate the value of this global structural damping ε, the experimental set-up is submitted to small amplitude vibrations at its free end. The displacements of the extremity are limited to small values to ensure that during the tests no fold is formed in the tape springs and their behaviour remains in the quasi-linear part described in Fig. 1. Compared to the experimental set-up in Fig. 3, the dummy appendix was replaced by an additional weight (Fig. 10) in order to reduce the frequency of these vibrations and improve the accuracy of the collected data.
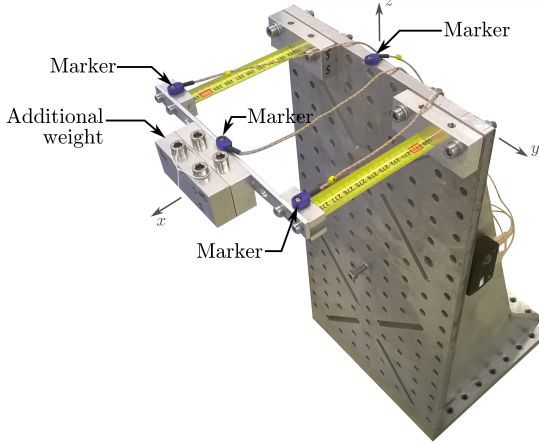
Figure 10: Experimental set-up used to perform small amplitude vibration tests and position of the markers.

The acquisition equipment consists of a 3D motion analysis system from CODAMOTION. For the small amplitude vibration tests, four active markers are placed on the set-up (Fig. 10) and four scanners from the CX1 series are located around the set-up. Each unit combines three motion sensing arrays and is then able to triangulate precisely the position of each marker (Fig. 11). The acquisition frequency of this system reaches $800\,Hz$ when less than six markers are used at the same time. This equipment is normally devoted to human motion analysis at the University of Liège, but is used here in a different context (see for example [26] for a more detailed description of the equipment and the analyses performed in the lab).

The results obtained with the small amplitude vibration tests are illustrated in Fig. 12 in terms of displacements around the equilibrium configuration. It can be seen that the damping of the oscillations tends to follow an exponential decay, which can be explained by the fact that the motion is dominated by the first bending mode in the case of small amplitude vibrations. Indeed, a modal analysis performed on the finite element model of the set-up shows that the structure is characterised by this first mode with an
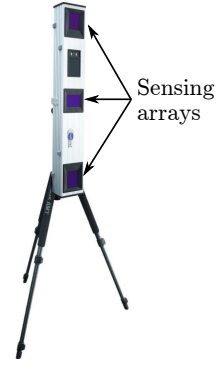

Figure 11: CODAMOTION CX1 unit.

eigenvalue of 10.52 Hz. The finite element model used here is more thoroughly described later in this section.
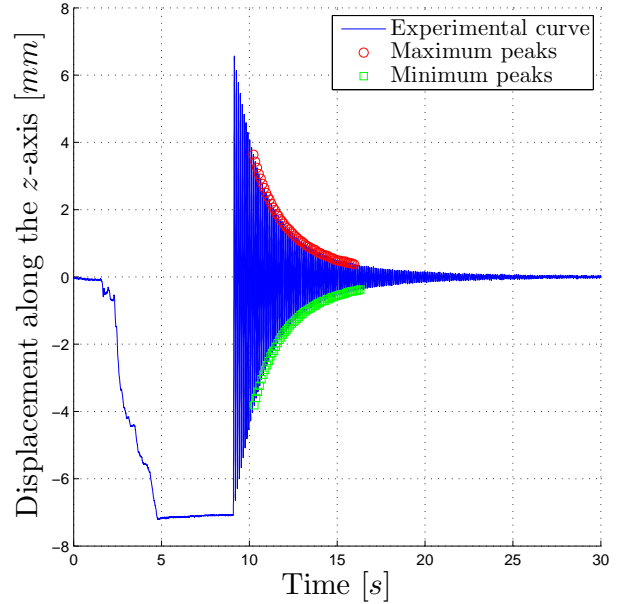

Figure 12: Experimental result of the small amplitude vibration tests.

Assuming then that the small amplitude vibrations follow an exponential decay, their theoretical evolution is illustrated in Fig. 13. The decay coefficient $-\varepsilon\omega_0$ is determined by fitting an exponential on the envelope of the curve defined by its maximum and minimum peaks, however, both the structural damping ε and the natural pulsation ω_0 are unknown. An additional equation is then required and is obtained by using the oscillation period Δt which can be linked to the two previous variables:

$$\Delta t = \frac{2\pi}{\omega_0\sqrt{1-\varepsilon^2}} \tag{2}$$

Experimentally, the tests are performed with an initial vertical displacement around $-8\,mm$ reached by applying a vertical load on the additional weight,
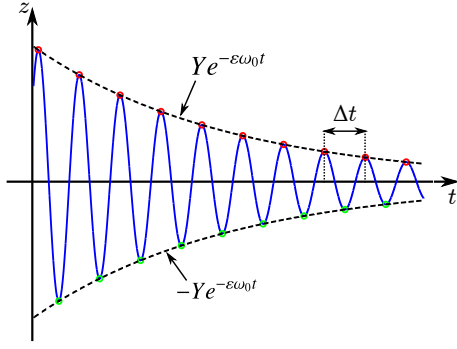
Figure 13: Theoretical evolution of the small amplitude vibrations in the case of an exponential decay.

nevertheless, only the peaks belonging to the intervals $\pm[4-0.4]$ mm are exploited. Indeed, displacements larger than 4 mm are too close from buckling and it cannot be assumed that the behaviour of the tape springs is still linear, while for displacements smaller than 0.4 mm, the experimental data are too altered by noise. The maximum and minimum peaks used to fit the exponentials and respecting these conditions are highlighted in Fig. 12.

In total, 510 small amplitude vibration tests were performed on 4 different pairs of tape springs during 11 sessions of tests. After each session, mean values were determined for both the structural damping ε and the oscillation period Δt. For information, it was not always possible to perform the same number of tests per session. The general mean on all the sessions are given in Tab. 8, along with the maximum difference noticed between sessions and the associated variation coefficient (relative standard deviation).

	Mean	Max. diff.	Variation coeff.
ε	0.509 %	0.288 %	20.67 %
Δt	0.100 s	0.003 s	0.919 %

Table 8: Experimental results from the small amplitude vibration tests with ε the structural damping and Δt the oscillation period (510 tests on 4 pairs of tape springs).

It can be concluded from Tab. 8 that the experimental measure of the structural damping ε is challenging, its value experiencing significant changes from one session of tests to another. Several elements were identified to explain this behaviour. First of all, the structural damping is sensitive to the assembly of the set-up. Indeed, between sessions, disassembling and re-building the set-up with the same tape springs showed variations in the mean structural damping. Furthermore, changing the tape springs also impacts that parameter since the measuring tape from which

they are cut out is probably not perfectly uniform. Finally, within a session of tests, the value of the structural damping tends to decrease as the number of tests increases as it can be seen in Fig. 14. This behaviour is most likely due to thermal effects, whose impact increases as the structure is more and more excited.
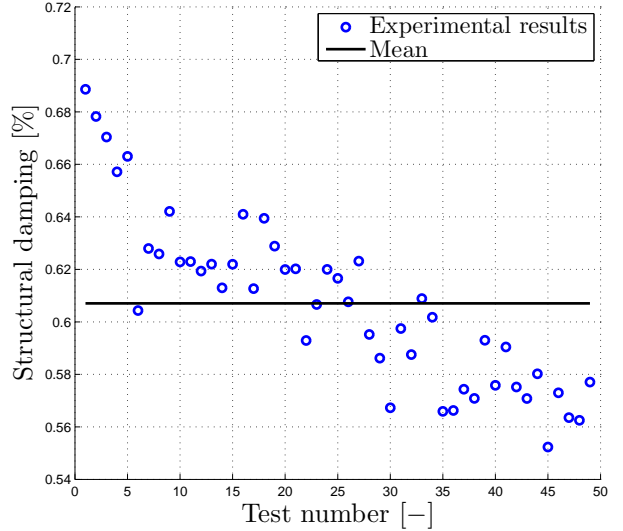

Figure 14: Thermal effects affecting the structural damping ε during the third session of small amplitude vibration tests.

Regarding the oscillation period Δt, this parameter is much less sensitive to all the disruptive elements mentioned previously and remains fairly stable between each session of tests.

Numerically, the small amplitude vibration tests are performed on the finite element model illustrated in Fig. 15 where the tape springs and the rod are represented with shell elements, while all the interfaces and the additional weight are considered as rigid volumes with the appropriate masses. The fixation support is not integrated in the model and the two big interfaces are then considered as clamped. As it was done experimentally, a vertical load is applied on the additional weight to reach the initial vertical displacement, then the structure is left free to oscillate. The solver used in this case is the generalised-α method of second order accuracy with low numerical damping [27].

To take into account the exponential decay of the small amplitude oscillations, the tape spring material is considered as a viscoelastic material in which the structural damping is defined by a Kelvin-Voigt model. This simple rheological model consists of a spring characterised by a stiffness k and a damper characterised by a viscosity η connected in parallel. Furthermore, in theory, the viscosity parameter η is
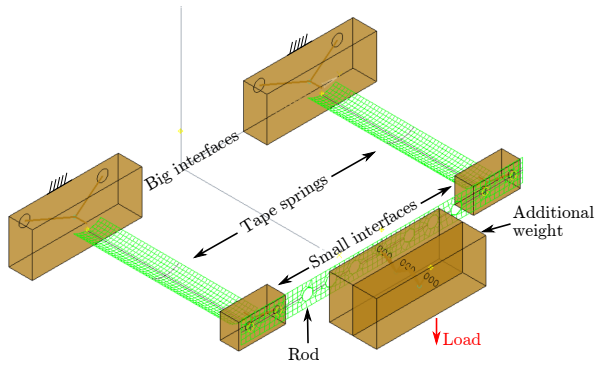
Figure 15: Finite element model used for the small amplitude vibration tests.

linearly related to the structural damping ε as:

$$\varepsilon = \frac{\eta}{2\omega_0 m} \tag{3}$$

where $\omega_0 = \sqrt{k/m}$ is the natural pulsation and m the mass.

In the case of the finite element model in Fig. 15, the linear relationship is preserved as illustrated in Fig. 16. Based on the linear interpolation and knowing the value of the structural damping ε, it is then possible to recover the equivalent viscosity parameter η to be used in the finite element model. The final numerical results are given in Tab. 9 and compared to the experimental ones. It can be seen that there is good agreement for both the structural damping ε and the oscillation period Δt.
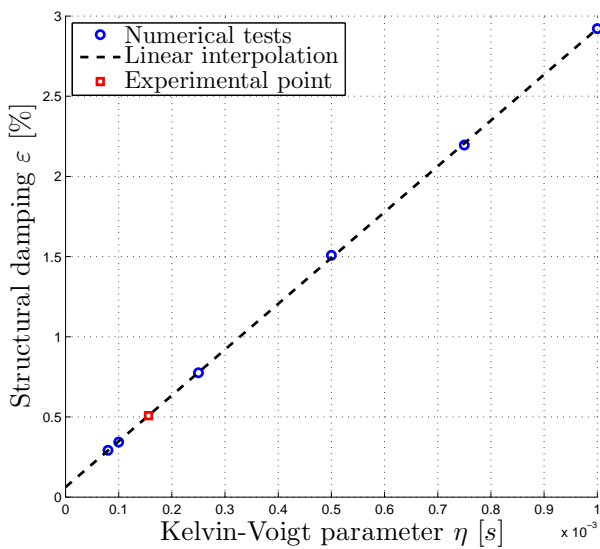
Figure 16: Relationship between the structural damping ε and the viscosity parameter η in the Kelvin-Voigt model.

	Exp.	Num.	Δ
ε	0.509 %	0.508 %	0.20 %
Δt	0.100 s	0.101 s	1.00 %
η	–	$1.56e^{-4}$ s	–

Table 9: Experimental and numerical results from the small amplitude vibration tests.

5 DEPLOYMENT TESTS

After having identified the parameters of the system, deployment tests are used to characterise the behaviour of the set-up in the case of large amplitude motion submitted to gravity. Initially, the tape springs are folded downwards in opposite sense as illustrated in Fig. 17 with an initial measured angle of 96.09° with respect to the horizontal. The mechanism is then set free by cutting a rope and left free to oscillate. In total, 170 deployment tests were performed on 4 pairs of tape springs during 4 sessions of tests. The acquisition equipment is the same as the one used for small amplitude vibration tests.
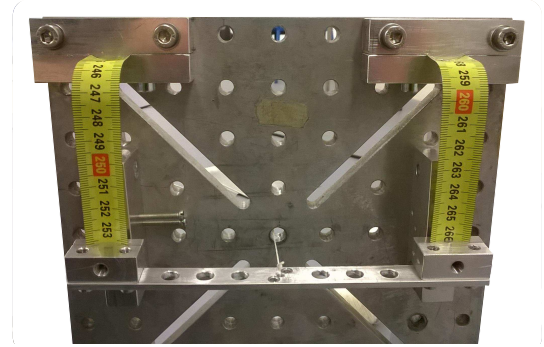

Figure 17: Initial folded configuration of the experimental set-up before deployment.

The results in terms of displacements along the x and z-axes obtained in the last session of tests are given in Figs. 18 and 19 respectively with the origin defined at the initial folded configuration. In this case, the displacements are measured in the middle of the rod and 50 curves are superimposed. It can be seen that the reproducibility of the tests is good for the first large peaks, but tends to deteriorate when the motion reaches smaller amplitudes.

In order to assess the quality of these experimental results, the variation coefficients (relative standard deviation) of the peak amplitude and the peak time are computed along each axis, x and z, for the ten first maximum and minimum peaks. It can be seen in Fig. 20 that the variation coefficient of the amplitude remains below 1 % for each peak, but as it was deduced from Figs. 18 and 19, that the variation co-
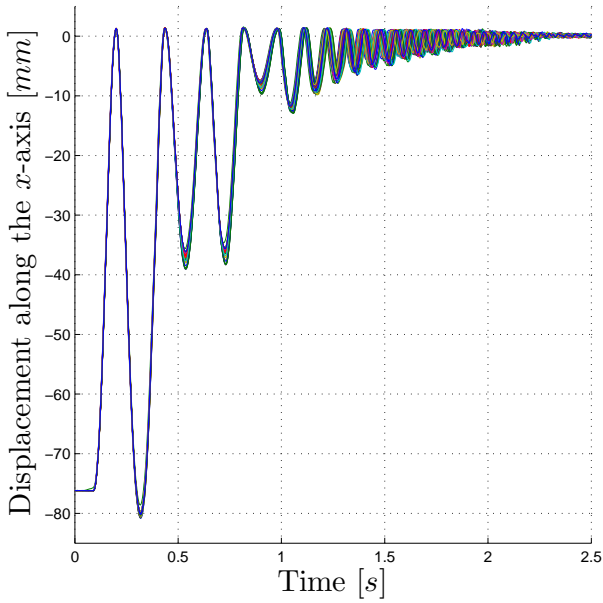
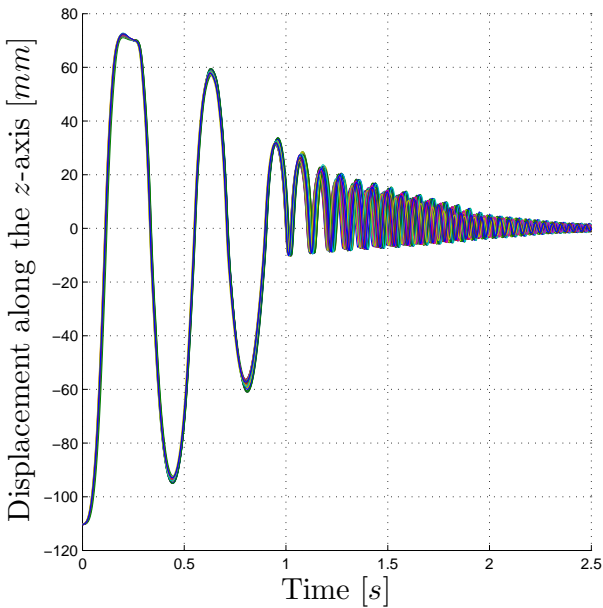Figure 18: Experimental displacements from the deployment tests along the x-axis.

Figure 19: Experimental displacements from the deployment tests along the z-axis.

Figure 20: Variation coefficients of the ten first experimental peaks in amplitude and time.

efficient of the time at which a peak occurs increases with the peak number. Notice that that time is defined as the elapsed time with respect to the instant of the first maximum peak, which explains why there is no value of variation coefficient at the peak number 1 for the blue ($-\circ-$) and green ($-\square-$) curves. In the end, the results shown in Fig. 20 allow then to validate the quality of the experimental measures. Furthermore, the lateral perturbations along the y-axis remain below 5.5 mm throughout the tests, showing that the use of a hinge composed of two tape springs limits torsion phenomena.
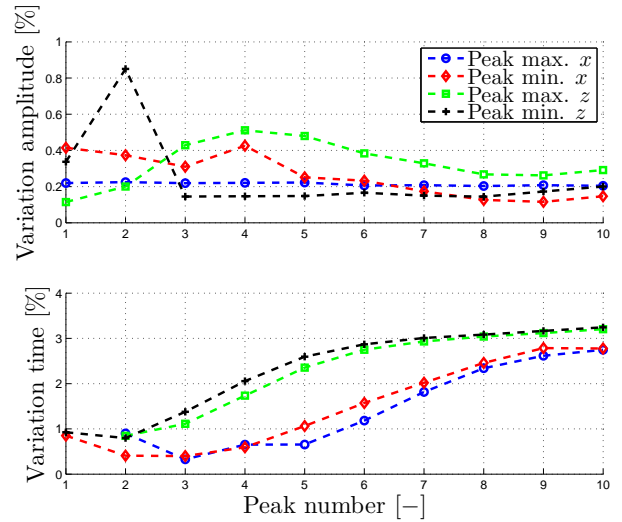
Numerically, the finite element model is folded in order for the middle of the rod to reach the same initial position than the one obtained experimentally, without any constraint on the folding angle as it was done on the set-up. This angle is measured afterwards at a value of 95.67°, that is a difference of .0.94 % with respect to the experimental one. The displacements along the x and z-axes are superimposed on the experimental results as dashed curves in Figs. 21 and 22 respectively. Qualitatively, it can be seen that the correlation is good along the z-axis except regarding the maximum peaks of small amplitude (Fig. 22). The same tendency is also noticed along the x-axis, but more importantly there is a large discrepancy on the amplitude of the first minimum peak (Fig. 21).

Quantitatively, the percentage of difference between the numerical and the mean experimental peaks in terms of amplitude and time is given in Fig. 23. As it was the case for the variation coefficients, there is no computed value regarding the difference of time for the first maximum peaks since they are used as references for all the others. Furthermore, the difference of amplitude in the case of the first minimum peaks is out of the visible range.

It can be concluded from these comparisons that the current finite element model gives fair results as their differences with respect to the experimental ones remain mostly below 15 %. Furthermore, as a reminder, the quasi-static results from the three points bending tests that allowed to determine the Young's modulus and the thickness were also in the same range of accuracy (see Section 3) with respect to the experimental data. It shows thus that extrapolating quasi-static results to perform dynamic analy-
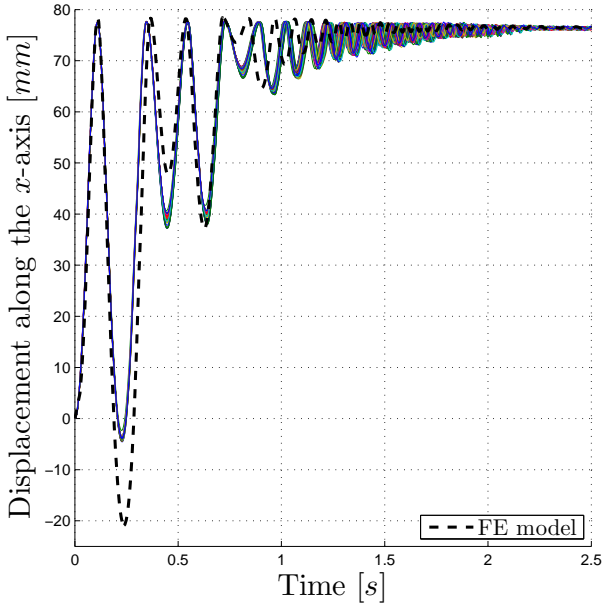
11

Figure 21: Comparison between the experimental and the numerical displacements during deployment along the *x*-axis.
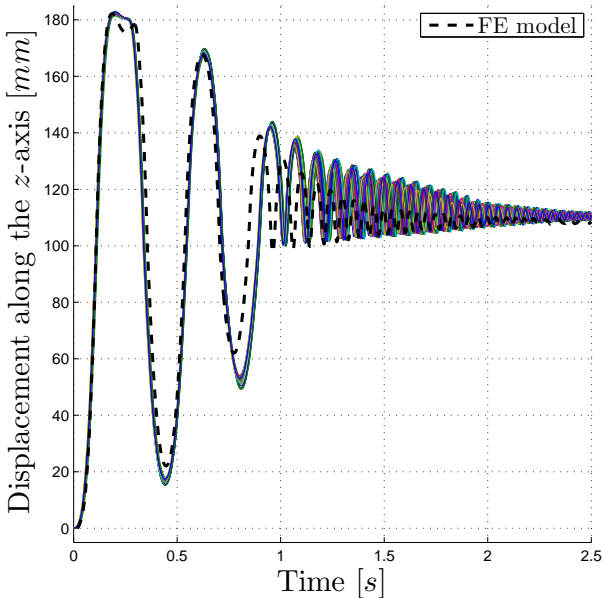

Figure 22: Comparison between the experimental and the numerical displacements during deployment along the *z*-axis.

ses is legitimate and is expected to be valid in simulation of deployments in space environment.

6 CONCLUSIONS

The purpose of this work is to collect experimental data on the highly nonlinear behaviour of tape springs in order to develop and validate an equivalent finite element model. To reach these objectives, an experimental set-up is first designed. This one con-
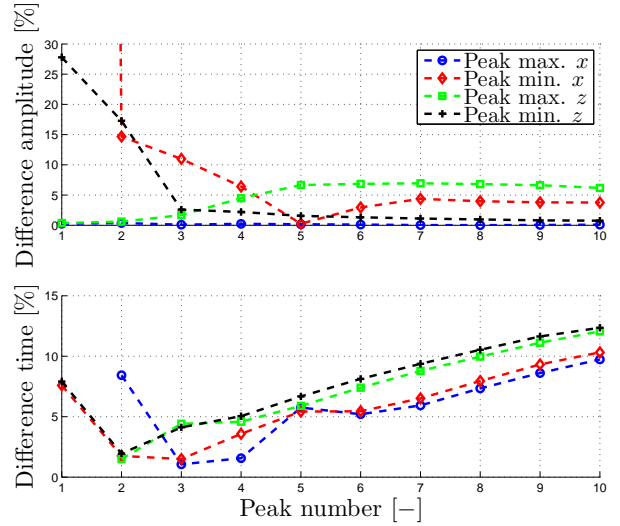

Figure 23: Percentage of difference between the amplitude and the time of the experimental and numerical peaks during deployment.

sists of two tape springs connected on one side to a fixation support and on the other one to a dummy appendix by the means of interfaces. Regarding the geometry and the material of the tape springs, uncertainties exist on the thickness and the Young's modulus. It limits then the acceptable mass at the free end of the set-up that leads to a passive deployment in both senses of bending.

To reduce the uncertainties on these two parameters, three points bending tests are performed on tape spring samples. The experimental results show a good reproducibility with a variation coefficient of less than 5 %. In order to determine the values of thickness and Young's modulus that fit at best the experimental data, the finite element model reproducing the three points bending tests is integrated in an optimisation procedure that leads, in the end, to numerical results deviating of less than 14 % from the experimental ones.

The next physical parameter to be determined is the structural damping of the whole structure, for which several sources are identified such as the flexibility of the tape springs, the connections between the different components or the air resistance. To quantify this parameter, small amplitude vibration tests are performed and captured by the means of a motion analysis system giving the evolution of the position of markers in real time. The experimental results show that the structural damping can experience relatively large changes from one session of tests to another, the global variation coefficient reaching 20 %. Several elements are identified to explain this behaviour: the sensitivity of the results to the assembly of the set-up and to the non-uniformity

of the measuring tape from which the tape springs are extracted, and thermal effects which tend to induce a decrease in the structural damping value as the structure is more and more excited. On the other hand, the oscillation period characterising the small amplitude vibrations remains stable throughout the different tests with a variation coefficient of less than 1 %. Numerically, the finite element model leads to results within 1 % of difference with respect to the experimental ones when a simple Kelvin-Voigt model is used to represent the structural damping in the tape springs.

Finally, the validity of the results is confirmed in deployment tests implying large amplitude motions. The experimental data still show a good reproducibility with a variation coefficient of less than 4 % on the analysed features, while the finite element model is able to reproduce them with differences mainly below 15 %, except for a limited number of points.

In future works, it would be interesting to further improve the correlation between the numerical and experimental results by, for example, exploiting more complex structural damping models. The experimental tests could also be completed by performing deployments with an initial bending in equal sense.

References

[1] J. Sicre, D. Givois, E. Emerit, Application of Maeva hinge to myriade microsatellites deployments needs, in: *11th European Space Mechanisms and Tribology Symposium (ESMATS) 2005, ESA/CNES*, Lucerne, Suisse, 21–23 September 2005.

[2] M. Mobrem, D. Adams, Deployment analysis of lenticular jointed antennas onboard the mars express spacecraft, *J. Spacecr. and Rockets* **46**, 2009, 394–402.

[3] K.A. Seffen, S. Pellegrino, Deployment of a rigid panel by tape-springs, *Department of Engineering, University of Cambridge, Report CUED/D-STRUCT/TR168.*, 1997.

[4] S. Pellegrino, Deployable Structures in Engineering, *Deployable Structures*, CISM Courses and Lectures, vol. 412, Springer (Wien), 2001.

[5] D. Givois, J. Sicre, T. Mazoyer, A low cost hinge for appendices deployment: design, test and application, in: *9th European Space Mechanisms and Tribology Symposium*, Liège, Belgium, 19-21 September 2001.

[6] C. Boesch, et al., Ultra light self-motorized mechanism for deployment of light weight space craft appendages, in: *39th Aerospace Mechanisms Symposium*, NASA Marshall Space Flight Center, 7-9 May 2008.

[7] H.M.Y.C. Mallikarachchi, S. Pellegrino, Quasi-static folding and deployment of ultrathin composite tape-spring hinges, *J. Spacecr. and Rockets* **48**, 2011, 187–198.

[8] K.A. Seffen, On the behaviour of folded tape-springs, *ASME J. Appl. Mech.* **68**, 2001, 369–375.

[9] K.A. Seffen, S. Pellegrino, Deployment dynamics of tape-springs, *Proc. R. Soc. Lond.* **A 455**, 1999, 1003–1048.

[10] W. Wüst, Einige Anwendungen des Theorie der Zylinderschale, *Z. Angew. Math. Mech.* **34**, 1954, 444–454.

[11] F.P.J. Rimrott, Querschnittsverformung bei Torsion offener Profile, *Z. Angew. Math. Mech.* **50**, 1970, 775–778.

[12] E.H. Mansfield, Large-deflexion torsion and flexure of initially curved strips, *Proc. R. Soc. Lond.* **A 334**, 1973, 1125–1132.

[13] F. Guinot, S. Bourgeois, B. Cochelin, L. Blanchard, A planar rod model with flexible thin-walled cross-sections. Application to the folding of tape springs, *Int. J. Solids Struct.* **49 (1)**, 2012, 73–86.

[14] F. Dewalque, J.-P. Collette, O. Brüls, Mechanical behaviour of tape springs used in the deployment of reflectors around a solar panel, *Acta Astronaut.* **123**, 2016, 271–282.

[15] S. Hoffait, O. Brüls, D. Granville, F. Cugnon, G. Kerschen, Dynamic analysis of the self-locking phenomenon in tape-spring hinges, *Acta Astronaut.* **66**, 2010, 1125–1132.

[16] F. Dewalque, P. Rochus, O. Brüls, Importance of structural damping in the dynamic analysis of compliant deployable structures, *Acta Astronaut.* **111**, 2015, 323–333.

[17] H.M.Y.C. Mallikarachchi, S. Pellegrino, Design of ultrathin composite self-deployable booms, *J. Spacecr. and Rockets* **51**, 2014, 1811–1821.

[18] A.J. Cook, S.J.I. Walker, Experimental research on tape spring supported space inflatable structures, *Acta Astronaut.* **118**, 2016, 316–328.

[19] S.J.I. Walker, G. Aglietti, Experimental investigation of tape springs folded in three dimensions, *AIAA J.* **44**, 2006, 151–159.

[20] Ö. Soykasap, Analysis of tape spring hinges, *Int. J. Mech. Sci.* **49**, 2007, 853–860.

[21] K.W. Kim, Y. Park, Systematic design of tape spring hinges for solar array by optimization method considering deployment performances, *Aerospace Science and Technology* **46**, 2015, 124–136.

[22] K. Kwok, S. Pellegrino, Viscoelastic effects in tape-springs, in: *52nd AIAA/ASME/ASCE/ AHS/ASC Structures, Structural Dynamics and Materials Conference*, Denver, CO, 4-7 April 2011.

[23] S.A. Samtech, SAMCEF User Manual, Version 8.4, 2013.

[24] N. Newmark. A method of computation for structural dynamics. *ASCE Journal of the Engineering Mechanics Division*, Vol. **85**, 67–94, 1959.

[25] The MathWorks, Matlab, 2009, Version 7.9.0 (R2009b).

[26] C. Schwartz, V. Denoël, B. Forthomme, J.-L. Croisier, O. Brüls, Merging multi-camera data to reduce motion analysis instrumental errors using Kalman filters, *Computer Methods in Biomechanics and Biomedical Engineering*, Taylor and Francis **18** (9), 952–960, 2015.

[27] J. Chung, G. Hulbert, A time integration algorithm for structural dynamics with improved numerical dissipation: the generalized-α method, *ASME J. Appl. Mech.* **60**, 1993, 371–375.